NASA Contractor Report 195014

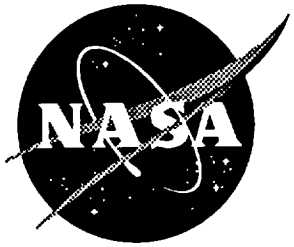

A Spectrally Accurate Boundary-Layer Code for Infinite Swept Wings

C. David Pruett
The College of William and Mary, Williamsburg, Virginia

Contract NAS1-19656
December 1994

National Aeronautics and
Space Administration
Langley Research Center
Hampton, Virginia 23681-0001

A Spectrally Accurate Boundary-Layer Code for Infinite Swept Wings

Dr. C. David Pruett
Program in Applied Science
The College of William and Mary

Abstract

This report documents the development, validation, and application of a spectrally accurate boundary-layer code, WINGBL2, which has been designed specifically for use in stability analyses of swept-wing configurations. Currently, we consider only the quasi-three-dimensional case of an infinitely long wing of constant cross section. The effects of streamwise curvature, streamwise pressure gradient, and wall suction and/or blowing are taken into account in the governing equations and boundary conditions. The boundary-layer equations are formulated both for the attachment-line flow and for the evolving boundary layer. The boundary-layer equations are solved by marching in the direction perpendicular to the leading edge, for which high-order (up to fifth) backward differencing techniques are used. In the wall-normal direction, a spectral collocation method, based on Chebyshev polynomial approximations, is exploited. Spectral accuracy is advantageous in that 1) the solution is highly accurate even for relatively coarse grids, 2) the boundary-layer profiles and their derivatives are extremely smooth, and 3) interpolation to other grids can be accomplished with virtually no loss of accuracy. The accuracy, efficiency, and user-friendliness of WINGBL2 make it well suited for applications to linear stability theory, parabolized stability equation methodology, direct numerical simulation, and large-eddy simulation. The method is validated against existing schemes for three tests cases, including incompressible swept Hiemenz flow and Mach 2.4 flow over an airfoil swept at 70° to the free stream.

1 Introduction

In the current global economy, the economic pressures on aircraft manufacturers are such that a single major design error could precipitate the financial collapse of an entire company. In such a competitive environment, the need for accurate, dependable, user-friendly, and robust numerical tools for analysis and design cannot be overemphasized.

In particular, the greater emphasis on drag reduction, transition prediction, and laminar-flow control technology highlights a current need for highly accurate boundary-layer codes. Although it is possible and might seem desirable to solve the full Navier-Stokes (NS) equations to obtain boundary-layer profiles for stability analyses, in practice, NS computations become prohibitively expensive whenever the boundary layer is highly resolved. (The reader should be aware that stability analyses require not only accurate determination of the mean flow but also of the first and second derivatives of mean-flow quantities; hence, accuracy requirements are stringent.) Consequently, current state-of-the-art techniques rely on boundary-layer calculations that are coupled to outer (inviscid) solutions obtained from the Euler equations. For the inner (boundary-layer) solution, spectral methods are particularly well suited. In practice, spectral accuracy guarantees extremely smooth boundary-layer profiles and ensures that derivatives and interpolants can be computed with no significant loss of accuracy.

This report documents a spectrally accurate boundary-layer code called WINGBL2, which was developed especially for application to analyses of crossflow instability and transition on highly swept wings (the dominant instability modes if the sweep angle is sufficiently large). In particular, WINGBL2 provides the boundary-layer profiles (and their derivatives) that are needed for linear stability analyses, for analyses based on parabolized stability equation (PSE) methodology, and for the base flow for direct numerical simulations (DNS) or large-eddy simulations (LES). Currently, we consider a quasi-three-dimensional geometry in which the wing is assumed to be infinitely long in span. The effects of surface curvature, streamwise pressure gradient, and wall suction and/or blowing are incorporated into the governing equations and boundary conditions. Because the code is intended for use by PSE, DNS, and LES, which consider mean-flow nonparallelism, particular attention is paid to the accurate determination of the wall-normal

velocity. Procedures for interpolation and extrapolation to other grids are also carefully addressed. The code is equally applicable to incompressible or compressible flows; however, because of the unnecessary participation of the energy equation in the incompressible limit, some performance penalty is incurred.

In the next section, we present the coordinate system and the governing equations for the infinite swept-wing geometry. In section 3, we introduce the boundary-layer transformations that lead to the transformed governing equations. The attachment-line boundary layer is considered as a special case. The numerical method is discussed in section 4. Section 5 treats evaluation of the wall-normal velocity. Data input and output are discussed in section 6, as are data interpolation and extrapolation to other grids. In section 7, we close with several validation test cases, among them incompressible swept Hiemenz flow and compressible flow over a highly swept wing.

2 Coordinate System and Boundary-Layer Equations

Let (x^*, y^*, z^*) be a body-oriented orthogonal coordinate system on a swept wing, where x^* is the arc length from the attachment line in the direction perpendicular to the leading edge, y^* is the wall-normal coordinate, and z^* is the spanwise coordinate parallel to the leading edge, as shown in Figure 1. (Throughout this report, dimensional quantities are denoted by an asterisk.) The body-fitted system is imbedded in a rectangular Cartesian coordinate system, which we denote by (l^*, r^*, z^*) and which will later be used to define the wing geometry. Consider the flow of air over the surface of the wing, where p^*, ρ^*, T^*, μ^*, and κ^* denote the pressure, density, temperature, viscosity, and thermal conductivity of the air, respectively. Furthermore, let $[u^*, v^*, w^*]^T$ denote the velocity vector in the (x^*, y^*, z^*) system.

The three-dimensional compressible boundary-layer equations are given in dimensional units for body-fitted coordinates on page 220 of reference [1]. Here, we impose two additional assumptions: the flow is laminar, and the span is infinite. The latter assumption implies that all terms that contain spanwise derivatives $(\frac{\partial}{\partial z^*})$ vanish. The following governing equations result:

Continuity:

$$\frac{\partial}{\partial x^*}(\rho^* u^*) + \frac{\partial}{\partial y^*}(q\rho^* v^*) = 0 \tag{1}$$

x-momentum:

$$\frac{\rho^* u^*}{q}\frac{\partial u^*}{\partial x^*} + \rho^* v^* \frac{\partial u^*}{\partial y^*} = -\frac{1}{q}\frac{\partial p^*}{\partial x^*} + \frac{\partial}{\partial y^*}\left(\mu^* \frac{\partial u^*}{\partial y^*}\right) \tag{2}$$

z-momentum:

$$\frac{\rho^* u^*}{q}\frac{\partial w^*}{\partial x^*} + \rho^* v^* \frac{\partial w^*}{\partial y^*} = \frac{\partial}{\partial y^*}\left(\mu^* \frac{\partial w^*}{\partial y^*}\right) \tag{3}$$

Energy:

$$\frac{\rho^* u^*}{q}\frac{\partial T^*}{\partial x^*} + \rho^* v^* \frac{\partial T^*}{\partial y^*} = \frac{\partial}{\partial y^*}\left(\frac{\mu^*}{Pr}\frac{\partial T^*}{\partial y^*}\right) + \mu^*\left(\frac{\partial u^*}{\partial y^*}\right)^2 + \mu^*\left(\frac{\partial w^*}{\partial y^*}\right)^2 \tag{4}$$

State:

$$p^* = \rho^* R_g^* T^* \tag{5}$$

where $Pr = \frac{\mu^*}{\kappa^*}$ is the Prandtl number, and R_g^* is the (ideal) gas constant.

In the equations above, one metric quantity, $q = 1 - y^* \frac{d\phi}{dx^*}$, arises from streamwise curvature, where $\phi = \tan^{-1}\frac{dr^*}{dl^*}$ is the angle in the (x^*, z^*) plane of the surface tangent to the body. In boundary-layer theory,

$$\frac{\partial p^*}{\partial y^*} = 0 \tag{6}$$

in which case we obtain

$$\frac{\partial p^*}{\partial x^*} = \frac{dp^*}{dx^*} = \rho_e^* u_e^* \frac{du_e^*}{dx^*} \tag{7}$$

for the inviscid flow. Throughout this paper, the subscript e denotes boundary-layer edge values.

3 Transformed Boundary-Layer Equations

Transformation of the boundary-layer equations is desirable for two reasons. First, Eqs. (1)–(4) are singular at $x^* = 0$. Second, a clever transformation will remove most of the timelike evolution in the x^* direction, which facilitates marching solutions. In accordance with reference [1], we adopt the transformation

$$\xi^* = x^* \tag{8}$$

$$\eta = \sqrt{\frac{u_e^*}{x^* \rho_e^* \mu_e^*}} \int_0^{y^*} \rho^* dy^* = \frac{1}{L^*} \int_0^{y^*} \theta^{-1} dy^* \tag{9}$$

where L^* is the boundary-layer length scale defined as

$$L^* = \sqrt{\frac{\mu_e^* x^*}{\rho_e^* u_e^*}} \tag{10}$$

and

$$\theta = \frac{\rho_e^*}{\rho^*} = \frac{T^*}{T_e^*} \tag{11}$$

is the equation of state under the boundary-layer approximation (Eq. (6)).

Three elements of the Jacobian of the transformation are readily accessible from Eqs. (8)–(9); these are

$$\frac{\partial \xi^*}{\partial x^*} = 1 \tag{12}$$

$$\frac{\partial \xi^*}{\partial y^*} = 0 \tag{13}$$

and

$$\frac{\partial \eta}{\partial y^*} = \frac{1}{L^* \theta} \tag{14}$$

Because the product of the Jabobian matrices of the forward and inverse transformations must be the identity matrix, we also ascertain

$$\frac{\partial x^*}{\partial \xi^*} = 1 \tag{15}$$

$$\frac{\partial y^*}{\partial \eta} = L^* \theta \tag{16}$$

and

$$\frac{\partial \eta}{\partial x^*} = -\frac{\partial \eta}{\partial y^*}\frac{\partial y^*}{\partial \xi^*} \tag{17}$$

From Eq. (16), we obtain

$$y^*(\xi^*, \eta) = L^*(\xi^*) \int_0^\eta \theta(\xi^*, \eta) d\eta \tag{18}$$

and

$$q(\xi^*, \eta) = 1 - L^*(\xi^*)\frac{d\phi}{d\xi^*} \int_0^\eta \vartheta(\xi^*, \eta) d\eta \tag{19}$$

3.1 Transformed Equations for $u_e^* > 0$

Provided that neither u_e^* nor w_e^* vanish, we can define dimensionless velocities as follows:

$$F = \frac{u^*}{u_e^*} \tag{20}$$

$$G = \frac{w^*}{w_e^*} \tag{21}$$

$$v = \frac{v^*}{u_e^*} \tag{22}$$

and

$$V = Re_L \frac{v}{\theta} + \frac{\xi^* F}{q}\frac{\partial \eta}{\partial x^*} \tag{23}$$

where Re_L is the Reynolds number based on L^*; that is,

$$Re_L = \frac{\rho_e^* u_e^* L^*}{\mu_e^*} \tag{24}$$

Note that $Re_L = \sqrt{Re_x}$. The following transformed governing equations result from Eqs. (1)–(4), transformation (8)–(9), and definitions (20)–(23):

Continuity:

$$\frac{\xi^*}{q}\frac{\partial F}{\partial \xi^*} + \frac{\partial V}{\partial \eta} + \frac{F}{2q}(1 + \beta_0) - \frac{\alpha_0}{\varsigma} V\theta = 0 \tag{25}$$

x-momentum:

$$\frac{\xi^* F}{q}\frac{\partial F}{\partial \xi^*} + V\frac{\partial F}{\partial \eta} - \frac{\beta_1}{q}(\theta - F^2) - \frac{\partial}{\partial \eta}\left[\tilde{\mu}\frac{\partial F}{\partial \eta}\right] = 0 \tag{26}$$

z-momentum:

$$\frac{\xi^* F}{q}\frac{\partial G}{\partial \xi^*} + V\frac{\partial G}{\partial \eta} - \frac{\partial}{\partial \eta}\left[\tilde{\mu}\frac{\partial G}{\partial \eta}\right] = 0 \tag{27}$$

Energy:

$$\frac{\xi^* F}{q}\frac{\partial \theta}{\partial \xi^*} + V\frac{\partial \theta}{\partial \eta} - \frac{\partial}{\partial \eta}\left[\frac{\tilde{\mu}}{Pr}\frac{\partial \theta}{\partial \eta}\right] - (\gamma-1)M_{u,e}^2\tilde{\mu}\left(\frac{\partial F}{\partial \eta}\right)^2 - (\gamma-1)M_{w,e}^2\tilde{\mu}\left(\frac{\partial G}{\partial \eta}\right)^2 = 0 \tag{28}$$

where

$$\alpha_0 = L^*\frac{d\phi}{d\xi^*} \tag{29}$$

$$\beta_0 = \frac{\xi^*}{\mu_e^*}\frac{d\mu_e^*}{d\xi^*} + \frac{\xi^*}{\rho_e^* u_e^*}\frac{d(\rho_e^* u_e^*)}{d\xi^*} \tag{30}$$

$$\beta_1 = \frac{\xi^*}{u_e^*}\frac{du_e^*}{d\xi^*} \tag{31}$$

$$M_{u,e} = \frac{u_e^*}{a_e^*}; \quad M_{w,e} = \frac{w_e^*}{a_e^*} \tag{32}$$

$$a_e^* = \sqrt{\gamma R g^* T_e^*} \tag{33}$$

and

$$\tilde{\mu} = \frac{\mu}{\theta}; \quad \mu = \frac{\mu^*}{\mu_e^*}; \quad \mu_e^* = \mu^*(T_e^*) \tag{34}$$

and where γ is the ratio of specific heats. For this work, we model viscosity (and thermal conductivity) by Sutherland's law, namely,

$$\mu(\theta) = \frac{\theta^{3/2}(1+C)}{\theta + C}; \quad C = \frac{198.6\mathrm{R}}{T_e^*} \tag{35}$$

Other viscosity laws are readily implemented.

Although all three velocity components appear above, the governing equations remain two dimensional in the sense that the flow variables are functions

of (ξ^*, η) only. The reader should be aware that the transformed continuity equation presented on page 397 of reference [1] is in error.

If the sweep angle $\psi = 0$, then w_e^* vanishes; however, Eqs. (25)–(28) remain valid if $G = 0$.

3.2 Attachment-Line Equations

When the body is blunt, the flow stagnates along the attachment line $\xi^* = 0$. By definition, $u_e^* = u^* = 0$ for $\xi^* = 0$, in which case the x-momentum equation vanishes. To borrow from the Frobenius method for singular differential equations, we differentiate Eq. (2) with respect to x^*; by then redefining F, V, and L^* as

$$F = \frac{f^*}{f_e^*}; \quad f^* = \frac{\partial u^*}{\partial x^*}; \quad f_e^* = \frac{du_e^*}{dx^*} \tag{36}$$

$$V = \frac{w_e^* v}{f_e^* L^* \theta} \tag{37}$$

and

$$L^* = \sqrt{\frac{\mu_e^*}{\rho_e^* f_e^*}} \tag{38}$$

we obtain an equation system formally identical to that of Eqs. (25)–(28), with the exception that the timelike derivative terms vanish and certain coefficients differ. Thus, the governing equations for $\xi^* = 0$ and for $\xi^* > 0$ can be put in the following universal form, valid for all ξ^* with proper interpretation of F, V, and L^*:

Continuity:

$$\frac{\xi^*}{q}\frac{\partial F}{\partial \xi^*} + \frac{\partial V}{\partial \eta} + \frac{C_{c1} F}{q} - \frac{C_{c2}}{q} V\theta = 0 \tag{39}$$

x-momentum:

$$\frac{\xi^* F}{q}\frac{\partial F}{\partial \xi^*} + V\frac{\partial F}{\partial \eta} - \frac{C_{x1}}{q}(\theta - F^2) - \frac{\partial}{\partial \eta}\left[\tilde{\mu}\frac{\partial F}{\partial \eta}\right] = 0 \tag{40}$$

z-momentum:

$$\frac{\xi^* F}{q}\frac{\partial G}{\partial \xi^*} + V\frac{\partial G}{\partial \eta} - \frac{\partial}{\partial \eta}\left[\tilde{\mu}\frac{\partial G}{\partial \eta}\right] = 0 \tag{41}$$

Energy:

$$\frac{\xi^* F}{q}\frac{\partial\theta}{\partial\xi^*} + V\frac{\partial\theta}{\partial\eta} - \frac{\partial}{\partial\eta}\left[\frac{\tilde{\mu}}{Pr}\frac{\partial\theta}{\partial\eta}\right] - C_{e1}\tilde{\mu}\left(\frac{\partial F}{\partial\eta}\right)^2 - C_{e2}\tilde{\mu}\left(\frac{\partial G}{\partial\eta}\right)^2 = 0 \quad (42)$$

If the body has a sharp leading edge or if $\xi^* > 0$, then

$$C_{c1} = \frac{1}{2}(1+\beta_0) \quad (43)$$

$$C_{c2} = \alpha_0 \quad (44)$$

$$C_{x1} = \beta_1 \quad (45)$$

$$C_{e1} = (\gamma - 1)M_{u,e}^2 \quad (46)$$

and

$$C_{e2} = (\gamma - 1)M_{w,e}^2 \quad (47)$$

Otherwise (if the body is blunt and $\xi^* = 0$), then

$$C_{c1} = 1 \quad (48)$$

$$C_{c2} = \alpha_0 \quad (49)$$

$$C_{x1} = 1 \quad (50)$$

$$C_{e1} = 0 \quad (51)$$

and

$$C_{e2} = (\gamma - 1)M_{w,e}^2 \quad (52)$$

3.3 Boundary Conditions

The appropriate wall boundary conditions for velocities are

$$F(0) = G(0) = 0; \quad V(0) = V_{\text{wall}} \quad (53)$$

where V_{wall} is negative for wall suction or positive for blowing. For the temperature at the wall, we consider either the isothermal condition

$$\theta(0) = \frac{T^*_{\text{wall}}}{T^*_e} \quad (54)$$

or the adiabatic-wall condition

$$\frac{\partial \theta}{\partial \eta} = 0 \tag{55}$$

At the far-field boundary $\eta = \eta_{\max}$

$$F = G = \theta = 1 \tag{56}$$

In the next section, a transformation will be introduced to eliminate the necessity of a far-field condition for V.

4 Numerical Methodology

Details of the spectral collocation method can be found in Pruett and Streett [2] and Pruett [3]. Here, we provide only a sketch of the method.

The governing equations (39)–(42) are solved by marching downstream in the timelike variable ξ^*. Timelike derivatives of the form $\frac{\partial F}{\partial \xi^*}$, for example, are approximated by high-order backward finite differences. The present code allows for mth-order differencing, where $1 \leq m \leq 5$. In practice, boundary-layer solutions are relatively insensitive to the order of the marching scheme; we recommend $m = 2$ or $m = 3$. The present scheme also permits equal or unequal steps in ξ^*. For the "initial condition" ($\xi^* = 0$), the timelike derivative terms vanish. For subsequent steps, the order of the scheme is limited initially by the number of previous stations available. That is, for step 1, $m = 1$; for step 2, $m = 2$, and so on, until the full order m of the scheme is established.

At each marching station ξ_i^* ($i = 0, 1, ..., M$), the solution procedure is equivalent to solving a system of four coupled nonlinear ordinary boundary-value problems in the variable η. As for finite-difference methods, we partition the domain such that $0 = \eta_0 < \eta_1 < ... < \eta_N = \eta_{\max}$, and we define the vectors $\vec{\theta}$, $\vec{F}$, $\vec{G}$, and $\vec{V}$, whose elements are the discrete approximations to their continuous counterparts at the $(N+1)$ grid points. Moreover, we define the discrete differentiation operator $[D]$, whereby, for example, $[D]\vec{\theta}$ approximates the continuous derivative $\frac{\partial \theta}{\partial \eta}$. Spectral accuracy is achieved by

approximating the continuous variables with finite expansions in the Chebyshev polynomials

$$T_j(\tilde{\eta}) = \cos\left[j \cos^{-1} \tilde{\eta}\right] \tag{57}$$

which are orthogonal on [-1,+1]. The natural (Gauss-Lobatto) set of collocation points associated with Eq. (57) is

$$\tilde{\eta}_j = \cos\frac{j\pi}{N} \quad (j = 0, 1, 2, ..., N) \tag{58}$$

for which the interpolating polynomial is uniformly bounded as $N \rightarrow \infty$. The differentiation operator $[D]$ is obtained by explicitly differentiating the Chebyshev polynomials at the collocation points. Unlike in standard finite-difference techniques, $[D]$ is a dense, rather than banded, $(N+1) \times (N+1)$ matrix. The advantage of spectral methods is that as $N \rightarrow \infty$ the truncation error diminishes faster than N^{-P} for any finite power P, a property known as spectral convergence. An additional advantage of spectral methods is that, unlike finite-difference methods, boundary points require no special treatment. Currently, we compute discrete derivatives by matrix multiplication, although a considerable performance gain can be realized for large values of N by fast Fourier transform methods.

For collocation methods, the discrete governing equations are required to be exactly satisfied at the collocation points. The discrete governing equations are analogous to their continuous counterparts (Eqs. (39)–(42)); for example, terms like $\frac{\partial V}{\partial \eta}$ become $[D]\vec{V}$. For initial guesses $\vec{\theta}^0$, $\vec{F}^0$, and so on, the four discrete governing equations define a residual vector $\vec{r}^0$ of length $4(N+1)$. The residual iterates $\vec{r}^k$, where k denotes the iteration index, are driven toward zero by Newton's method. The Jacobian for Newton's method is a nearly dense $[4(N+1)] \times [4(N+1)]$ matrix. For $i > 0$, the starting values for the iteration are obtained from the converged solution of the previous marching step. For spectral methods based on Chebyshev polynomials, Jacobians are typically quite ill-conditioned. Typically six to seven iterations are required to drive the norm of the residual vector to 10^{-7}, a level at which the solution is smooth to nearly machine precision. To obtain convergence of the iteration, all dependencies must be represented by the Jacobian, including, for example, the variation of q with θ implicit in Eq. (19).

In practice, before the discrete equations are solved, we make one further transformation to Eq. (39). By multiplying the continuity equation by q and

integrating both sides from η_{j-1} to η_j, we obtain

$$qV|_{\eta_j} - qV|_{\eta_{j-1}} + \int_{\eta_{j-1}}^{\eta_j} \left[C_{c1} F + \xi^* \frac{\partial F}{\partial \xi^*} \right] d\eta = 0 \quad (j = 1, ..., N) \qquad (59)$$

Integration of Eq. (39) has two advantages. First, after integration, no boundary condition is needed for V_N (which is now part of the solution). Second, a term produced in the integration by parts of $q\frac{\partial V}{\partial \eta}$ exactly cancels the term that contains C_{c2} in Eq. (39). The discrete integration that corresponds to the integral in Eq. (59) is also performed by the method described in [3], which makes use of a spectrally accurate quadrature operator $[Q]$ in the form of an $N \times (N+1)$ matrix.

One final practical consideration requires the use of a continuous transformation $\eta(\tilde{\eta})$ from the computational domain [-1,+1] to the physical domain $[0, \eta_{\max}]$. A well-designed transformation also serves to concentrate points near the wall, as is desirable for boundary-layer calculations. The reader is referred to reference [3] for details of the specific transformation. In practice, the metric $\partial\tilde{\eta}/\partial\eta$, computed either analytically or numerically to spectral accuracy, is imbedded directly into the differentiation and quadrature operators $[D]$ and $[Q]$, respectively.

5 Spectrally Accurate Extraction of Wall-Normal Velocity

Historically, the wall-normal v velocity has been the stepchild of boundary-layer approximations. Until recently, most stability analyses for boundary-layer flows assumed the mean flow to be locally parallel, in which case the wall-normal velocity was disregarded altogether. With the advent of multiple-scales analyses, PSE methodology, and spatial DNS, each of which considers mean-flow nonparallelism, the wall-normal velocity has assumed greater importance. This is particularly true for high-speed flows, in which nonparallel effects can be quite important. When desired, the wall-normal velocity is usually extracted from the continuity equation in physical space; this process requires interpolation, which can result in poor accuracy. In accordance with Pruett [3], a better approach is to extract v directly from the

transformations (23) and (37), in which case the continuity equation remains as a check.

From Eqs. (23) and (37), respectively, we obtain

$$v = \frac{\theta}{Re_L}\left[V - \frac{\xi^* F}{q}\frac{\partial \eta}{\partial x^*}\right] \quad (\xi^* \neq 0) \tag{60}$$

$$v = \frac{f_e^* L^*}{w_e^*} V\theta \quad (\xi^* = 0, \text{ blunt body}) \tag{61}$$

The extraction of v is straightforward for the attachment-line problem $\xi^* = 0$. However, for $\xi^* \neq 0$, Eq. (60) requires an expression for $\frac{\partial \eta}{\partial x^*}$. By explicitly differentiating transformation (9) with respect to x^*, we obtain

$$\theta\frac{\partial \eta}{\partial x^*} = -\int_0^\eta \theta_\xi d\eta - \frac{y^*}{2L^*}\left[\frac{1}{\xi^*} - \frac{1}{Re_1}\frac{d(Re_1)}{d\xi^*}\right] \tag{62}$$

where $Re_1 = \rho_e^* u_e^*/\mu_e^*$ is the edge unit Reynolds number. To obtain Eq. (62), we have used Leibniz' Rule to differentiate Eq. (9) beneath the integral sign. The integrations necessitated by the first term in Eq. (62) and y^* (see Eq. (18)) in the second term of Eq. (62) are computed to spectral accuracy by the integration procedure described in detail in reference [3].

6 Code Input and Output

6.1 Input

Four input files are required to define the physical parameter values, the parameters of the method, the geometry, and the boundary-layer edge data. Physical constants are set in a file "constants.h," which is incorporated into subroutine "econ1.f" by a FORTRAN include statement. This file normally resides with the source code. Default values are supplied for any physical constants not specified. Parameters of the method are read from standard input (FORTRAN unit 5) in the initialization subroutine "init.f." We have named the standard input file "wingbl2.d." The wing geometry is specified in file

"geom.dat" and read by subroutine "sgeom1.f," which uses cubic splines to obtain accurate interpolated values for ξ^*, ϕ, and so on. The boundary-layer edge data are specified in file "edge.dat" and read by subroutine "econ1.f," in which splines are also exploited for accurate interpolation of the edge data. Sample listings of the input data files are provided in appendix A. These files and the source code are documented such that the role of most parameters is self-explanatory. In the following subsections, we provide additional documentation for those parameters whose usage is not self-evident.

6.2 Determination of Arc Length

File "geom.dat" contains the chord length c^* (CHORD), the sweep angle ψ in degrees (SWEEPD), a parameter KSPLIT, whose function will soon become evident, and tabulated values of l^*/c^* and r^*/c^*, which define the wing geometry relative to some origin whose precise coordinates are unimportant. If the parameter CHORD is negative, the negative sign is interpreted to mean that the chord length c_n^* (normal to the leading edge) has been specified in lieu of c^* (chord length parallel to the free-stream velocity vector). On the basis of Figure 1, the relationship between these two values is $c_n^* = c^* \cos\psi$. For the case (CHORD < 0), the tabulated values l^* and r^* are assumed to be normalized by c_n^*.

Considerable care was devoted to ensure that geometric and edge data are evaluated accurately. Specifically, to avoid singularities in the calculation of arc length, we employ the two equivalent expressions

$$\xi^*(l^*) = \int_0^{l^*} \sqrt{1 + \left(\frac{dr^*}{dl^*}\right)^2}\, dl^* \tag{63}$$

and

$$\xi^*(r^*) = \int_0^{r^*} \sqrt{1 + \left(\frac{dl^*}{dr^*}\right)^2}\, dr^* \tag{64}$$

where Eq. (59) is used in the attachment-line region and Eq. (60) is used elsewhere. The switch from Eq. (59) to (60) is made at grid point KSPLIT (an input parameter referred to above), typically near the point at which $dr^*/dl^* = 1$. The integrands on the different regions are independently fit

with splines, and the resulting spline functions are integrated analytically. To ensure continuity of first and second derivatives at the interface, the end conditions on the matching splines are adjusted as follows. It can be determined from elementary calculus that

$$\frac{dr^*}{dl^*} = \frac{1}{dl^*/dr^*} \tag{65}$$

and

$$\frac{d^2r^*}{dl^{*2}} = -\left(\frac{dr^*}{dl^*}\right)^3 \frac{d^2l^*}{dr^{*2}} \tag{66}$$

An initial guess is made for $\frac{d^2r^*}{dl^{*2}}$ as an end condition for one spline; the other end condition is determined from Eq. (66). The assumed value is subsequently adjusted with the secant method until Eq. (65) is satisfied. At convergence, functional values and first and second derivatives are consistent at the interface.

Similarly, ϕ and $\frac{d\phi}{d\xi^*}$ are obtained from two different sets of expressions:

$$\phi = \text{ATAN2}(\frac{dr^*}{dl^*}, 1.); \quad \frac{d\phi}{d\xi^*} = \cos^3\phi \frac{d^2r^*}{dl^{*2}} \tag{67}$$

$$\phi = \text{ATAN2}(1., \frac{dl^*}{dr^*}); \quad \frac{d\phi}{d\xi^*} = -\sin^3\phi \frac{d^2l^*}{dr^{*2}} \tag{68}$$

where ATAN2 is a particular two-argument FORTRAN arctan function.

6.3 Gas Relations for Edge Conditions

Our interest is in high-efficiency wings without shocks. Consequently, we assume that the flow is isentropic and that the fluid is a perfect gas. (It is straightforward, however, to modify the gas relations to consider non-isentropic flow.) From file "edge.dat," we obtain the free-stream Mach number M_∞ (MINF), the pressure p^*_∞ (PINF), and the temperature T^*_∞ (TINF), as well as tabulated values of the chordwise coordinate l^*/c^* (XC) (scaled either by c^* or c^*_n), the pressure coefficient Cp_e (PC), and the suction coefficient Cq_e (QC). From this data, the total free-stream velocity U^*_∞ (UTINF) is computed as

$$U^*_\infty = M_\infty \sqrt{\gamma R g^* T^*_\infty} \tag{69}$$

Edge pressure data are extracted from the pressure coefficients (PC) as

$$Cp_e = \frac{p_e^* - p_\infty^*}{\frac{\gamma}{2} p_\infty^* M_\infty^2} \tag{70}$$

From Eq. (70), we obtain

$$\frac{p_e^*}{p_\infty^*} = 1 + \frac{\gamma}{2} Cp_e M_\infty^2 \tag{71}$$

From the isentropic perfect gas relations given in reference [4], we obtain

$$\frac{T_e^*}{T_\infty^*} = \frac{p_e^*}{p_\infty^*}^{\frac{\gamma-1}{\gamma}} \tag{72}$$

and

$$\left(\frac{U_e^*}{U_\infty^*}\right)^2 = 1 + \frac{2}{(\gamma-1)M_\infty^2}\left[1 - \frac{T_e^*}{T_\infty^*}\right] \tag{73}$$

For the infinite swept wing, the spanwise edge velocity is constant, namely,

$$w_e^* = U_\infty^* \sin\psi \tag{74}$$

From Eqs. (73)–(74) and the expression

$$U_e^* = \sqrt{u_e^{*2} + w_e^{*2}} \tag{75}$$

we obtain u_e^*. The contribution of the wall-normal velocity to the total velocity is assumed to be inconsequential. Given these quantities, the variations along the boundary-layer edge of all other quantities of interest (e.g., Reynolds number) readily follow. Two additional parameters head file "edge.dat." These are IFIRST, which relates the first indices of the tabulated values of files "geom.dat" and "edge.dat," and ISTAG, which identifies the index of the stagnation point (attachment line). At present, the tabulated locations l^*/c^* of "edge.dat" are assumed to be a contiguous subset of the values listed in "geom.dat." Furthermore, the stagnation point is assumed to be known. However, the spline interpolation algorithms are quite general, and these restrictions are easily relaxed.

6.4 Wall Suction

From the tabulated suction coefficients Cq_e (QC), we derive values for V_{wall} as follows. From the definition

$$Cq_e = \left[\frac{\rho^* v^*_{\text{wall}}}{\rho^*_\infty U^*_\infty}\right] \tag{76}$$

we obtain either

$$\frac{v}{\theta}|_{\text{wall}} = \frac{\rho^*_\infty U^*_\infty}{\rho^*_e u^*_e} Cq_e \tag{77}$$

for $u^*_e \neq 0$ or

$$\frac{v}{\theta}|_{\text{wall}} = \frac{\rho^*_\infty U^*_\infty}{\rho^*_e w^*_e} Cq_e \tag{78}$$

for attachment-line flow. From Eqs. (77) and (78) above and Eqs. (23) and (37), appropriate expressions for V_{wall} are readily obtained. (Note that Eq. (23) simplifies considerably at the wall because $\frac{\partial \eta}{\partial x^*}$ vanishes there.)

6.5 Output

The output consists of a file "legend" and a collection of numbered files beginning with "sta_0000" and numbered with increments of IOUT (an output parameter), all placed in subdirectory "sta" (for "stations"). Each "sta_xxxx" file corresponds to a particular value of x^* and contains the dimensionless quantities θ, F, G, and v and their first and second derivatives with respect to y. Appended at the end of each "sta_xxxx" file is a list of approximately 30 relevant dimensional and dimensionless values that apply at the given station, among them x^*, local Mach number, Reynolds number, displacement thickness, and boundary-layer edge conditions. The file "legend" tabulates summary information from the "sta_xxxx" files. Sample "legend" and "sta_xxxx" files are given in appendix B. Lengths in the output files are nondimensionalized at the user's option (ISCALE) either by the boundary-layer length scale L^* (Eq. (10)) or by the boundary-layer displacement thickness δ^*, which is defined as

$$\delta^* = \int_0^\infty \left[1 - \frac{\rho^* u^*}{\rho^*_e u^*_e}\right] dy^* = L^* \int_0^{\eta\text{max}} [\theta - F]\, d\eta \tag{79}$$

Among the quantities tabulated in the "legend" file are δ^* and the ratio δ^*/L^* as functions of x^*. As the Mach number increases, the ratio δ^*/L^* increases dramatically from its value of about 1.7 at $M_\infty = 0$. Consequently, δ^* is the more practical length scale, although L^* is the conventional scale in stability theory. A recommended rule of thumb is to adjust $\eta_{\max}$ (ETA_MAX, an input parameter) to ensure that the computational domain is at least $3\delta^*$ in thickness. Otherwise, the outer boundary condition will "pinch" the solution.

In addition to the output described above, several diagnostic files are produced; among these is the standard output file to FORTRAN unit 6.

6.6 Interpolation and Extrapolation

Because the present code is designed specifically for applications to stability analyses, DNS, and LES, we have paid special attention to the process of interpolating and extrapolating data to other grids. For this purpose, a companion code INTBL has been written. In brief, the procedure is as follows. In the output from WINGBL2, lengths are scaled either by L^* or δ^*, each of which grows with x^*. The outer edge of the boundary layer typically lies between 2 and 4 displacement thicknesses from the wall. Let $y_e(x^*)$ denote the location of the boundary-layer edge, where $y = y^*/L^*$. To interpolate to a grid that is uniform in y, for example, we first perform spectrally accurate interpolation in the interior region ($0 \le y \le y_e$) coupled with analytic extrapolation outside the boundary layer ($y > y_e$). This step is followed by high-order (typically fifth) polynomial interpolation in x^*.

Analytical extrapolation of u^*, T^*, and w^* is trivial because, for example, $u^* = u_e^*$ in the outer flow. Extrapolation of v^*, however, requires some care. From the continuity equation (Eq. (1)), we derive the following ordinary differential equation for the far-field behavior of v:

$$(1 - \alpha_0 y)\frac{dv}{dy} - \alpha_0 v = -\beta \tag{80}$$

where α_0 and v are defined in Eqs. (29) and (22), respectively, and

$$\beta = \frac{L^*}{\rho_e^* u_e^*}\frac{d(\rho_e^* u_e^*)}{dx^*} \tag{81}$$

Equation (80) has the exact solution

$$v(y) = v_e \left[\frac{1-\alpha_0 y_e}{1-\alpha_0 y}\right] - \beta \left[\frac{y-y_e}{1-\alpha_0 y}\right] \tag{82}$$

where $v_e = v(y_e)$. From Eq. (82), we also obtain $v'(y)$ and $v''(y)$.

7 Code Validation

We present three test cases that collectively validate WINGBL2 for compressible and incompressible flows, for two-dimensional and quasi-three-dimensional flows, and for flows over bodies with and without streamwise curvature and with and without streamwise pressure gradients.

7.1 Two-Dimensional Compressible Flow Along a Flat Plate

Here, we consider a two-dimensional Mach 4.5 flow of air along a flat plate with a sharp leading edge. For a thin plate and a thin boundary layer, the shock is oblique and weak and the flow can be considered to be approximately isentropic. The parameters of the flow are $M_\infty = 4.5$, $T_\infty = 110°\mathrm{R}$, $Re_1 = 2.888 \times 10^6$, $\gamma = 1.4$, and $Pr = 0.7$. The pressure and the suction coefficients are zero. The geometric parameters are $\psi = 0$, with a sharp leading edge (IBLUNT=0) and no streamwise curvature ($r^*(l^*) = 0$). In the absence of a streamwise pressure gradient, a similarity solution exists. Figure 2 compares results from the present code with those obtained from the spectrally accurate boundary-layer code of Pruett and Streett [2]. Results from the two methods are indistinguishable.

7.2 Incompressible Swept Hiemenz Flow

The incompressible swept Hiemenz problem, which was studied thoroughly in Malik et al. [5], represents an idealized stagnation-region flow on a swept

flat plate. In the absence of body curvature, u_e^* varies linearly with x^* (i.e., du_e^*/dx^* is constant), and a similarity solution exists for which the boundary-layer thickness remains fixed with x^*. The reader is referred to reference [5] for details of the problem and the geometry. Figure 3 presents the results obtained by the present method with those of reference [5] at a station x^* for which $Re_L = 500$ and $u_e^* = w_e^*$. The results of the two methods are indistinguishable. Results for incompressible flow were obtained from the present code by setting $M_\infty = 0.01$, $p_\infty^* = 2000$ psf, and $T_\infty^* = 520°$R, and by adjusting the velocity gradient du_e^*/dx^* and the sweep angle ψ to obtain $Re_L = 500$ and $u_e^* = w_e^*$ at some arbitrary value of x^*. The parameters selected were $\psi = 50.7°$ and $du_e^*/dx^* = 0.0961$ sec^{-1}, which gave $x^* = 90$ ft as the station of interest. We point out that for the present method the algorithm actually switches from the attachment-line equations to the equations of the evolving boundary-layer flow; however, the solutions are virtually identical, as they should be for this unique problem.

7.3 Flow on a Supersonic, Highly Swept Wing

Here, we compute the boundary layer on the upper surface of an infinitely long shockless wing with a chord length 20 ft; the wing is swept 70.22° to a free-stream velocity of Mach 2.4. The input files presented in appendix A contain the data for this test case (condensed for brevity). This case represents a stringent test for boundary-layer codes. Streamwise curvature in the attachment-line region is quite strong, and regions of both favorable and adverse pressure gradients exist. The maximum Mach number attained in the direction perpendicular to the wing is about 0.95, in which case a shock is avoided and isentropic gas relations apply. Figures 4 (a,b,c) compare the present results with those obtained from the code of Wie [6] at stations $x^* = 6.9\times10^{-3}$, 0.851, and 4.027 ft, respectively. For both the finite-difference and spectral methods, approximately 40 grid points were used across the boundary layer. The agreement is good at all three stations, except for some disagreement in the wall-normal velocity. Both solutions fail to converge for $l^*/c^* > 0.6$, where there is a strong adverse pressure gradient. With strong suction in the trailing-edge region, the present code predicts that attached flow can be maintained. To obtain a solution for $l^*/c^* > 0.6$ without suction, interaction must be allowed between the inviscid region and the boundary layer. In Figure 5, we compare second derivatives of the u-velocity component

at station $x^* = 4.027$ ft. The agreement is quite good.

For applications to stability analyses, we prefer to use approximately 100 points across the boundary layer, even for the spectral method. Such fine resolution is unnecessary but desirable for two reasons. First, for the present spectral method with $N = 100$, the velocity and temperature profiles and their first and second derivatives are smooth to 13, 10, and 7 significant digits, respectively. For stability analyses, the smoothness of the profiles and their derivatives, in addition to accuracy, is important. Second, a high-density grid ensures virtually no loss of accuracy in interpolation to other grids.

In summary, the present method is well suited for stability analyses that use any of the following numerical tools: LST, PSE, DNS, or LES. The spectral accuracy of the present scheme and its accurate determination of the wall-normal velocity render WINGBL2 particularly attractive for application to high-speed boundary-layer flows, which are quite sensitive to subtle changes in the mean state.

Acknowledgments

The author is grateful to Drs. Craig Streett and Chau-Lyan Chang for many helpful discussions and physical insights.

References

[1] D. A. Anderson, J. C. Tannehill, and R. H. Pletcher, *Computational Fluid Mechanics and Heat Transfer*, Taylor and Francis, New York, 1984, pp. 220, 396-398.

[2] C. D. Pruett and Craig L. Streett, "A Spectral Collocation Method for Compressible, Non-similar Boundary Layers," *Int. J. Numer. Meth. Fluids*, **13**, 6, 1991, pp. 713-737.

[3] C. D. Pruett, "On the Accurate Prediction of the Wall-Normal Velocity in Compressible Boundary-Layer Flow," *Int. J. Numer. Meth. Fluids*, **16**, 1993, pp. 133-152.

[4] Ames Research Staff, "Equations, Tables, and Charts for Compressible Flow," NACA Report 1135, 1965.

[5] M. R. Malik, F. Li, and C.-L. Chang, "Crossflow Disturbances in Three-Dimensional Boundary Layers," *J. Fluid Mech.*, **268**, 1994, pp. 1-36.

[6] Y.-S. Wie, "BLSTA–A Boundary Layer Code for Stability Analysis," NASA CR-4481, 1992.

Appendix A: Input Files

Input file "constants.h"

```
rgas = 1716.
co1 = 2.27e-8
co2 = 198.6
pr = 0.72
gamma = 1.4
```

Input file "wingbl2.d"

```
 1      /IBLUNT = 0 (sharp leading edge); 1 (blunt body)
 0      /ISCALE = 0 (scale lengths by L*); 1 (scale by delta*)
 60     /NSTEPS = number of steps in marching (xi) direction
-0.05   /DX = dimensional increment in x if > 0 (otherwise use input grid)
 42     /NP = N+1 = number of grid points in wall-normal (eta) direction
 0      /ISTART = start switch: 0 (fresh start); i > 0 (restart from i)
 3      /M = max. order of backward difference method [2 or 3 RECOMMENDED]
 1      /IOUT = output stride for sta_xxxx files
 5.e-7  /RLIM = maximum residual allowed  [KEEP DEFAULT 5.e-7]
 20     /ITMAX = iteration limit  [KEEP DEFAULT 20]
 0.7    /STR = parameter of tanh stretching  [KEEP DEFAULT 0.7]
 12.0   /ETA_MAX = outer bound in wall-normal variable eta
 -.35   /RO = initial guess for F = 1 - exp(ro*eta)  [KEEP DEFAULT -.35]
 300.   /TWALL = dimensional wall temp. (Rankine--irrelevant for iadiab=1)
 1      /IADIAB = wall boundary condition:  0 (isothermal); 1 (adiabatic)

notes:  1) to run, create the subdirectory /sta

        2) input files needed

           'geom.dat'     geometry data
           'edge.dat'     boundary-layer edge data
           'wingbl2.d'    standard input containing parameters of
                          method

        3) for cubic spline interpolation, edge data file must have
           at least 4 points

        4) at completion, subdirectory /sta will contain

           file 'legend'
           nsteps/iout numbered files 'sta_xxxx'
```

Input file "geom.dat"

```
20 /number of descriptive header records
#
#####################################################################
#
#   title:  SUPERSONIC SWEPT-WING CASE
#
#   airfoil:  NACA16006
#
#   geometry data:
#
#         CHORD:   chord length (c*) if > 0
#                  or normal chord (c_n*) if < 0
#         SWEEPD:  sweep angle (psi) in degrees
#         KSPLIT:  index at which to switch from
#                  Eq. (63) to Eq. (64)
#
#         tabular values of length l* and r* normalized
#                  by c* or c_n* according to value of CHORD
#
#####################################################################
#
20.0000         /chord
70.2180970318   /sweepd
8               /ksplit
 2.9971707E-3    -1.0969796405742E-3
 1.8810658E-3    -8.7168943307489E-4
 9.4530382E-4    -6.2043138039564E-4
 2.6244059E-4    -3.2962356850761E-4
 0.               0.
 2.6244059E-4     3.2962356850761E-4
 9.4530382E-4     6.2043138039564E-4
 1.8810658E-3     8.7168943307489E-4
 2.9971707E-3     1.0969796405742E-3
                .
                .
                .
 0.9824749        1.0061736003393E-3
 0.9865789        7.8976675042668E-4
 0.9903595        5.7946564411269E-4
 0.9938442        3.7687616857631E-4
 0.9970505        1.8348090931462E-4
 1.               0.
```

Input file "edge.dat"

```
9 /number of descriptive header records
#
#####################################################################
#
#         Freestream data, pressure and suction coefficients
#
#         tabular values of normalized length l*, cp_e, cq_e
#
#####################################################################
#
5       /ifirst (index in 'geom.dat' corresponding to first point)
1       /istag  (index of stagnation point/attachment line)
2.4     /rminf  (freestream Mach number)
149.76 /pinf    (freestream pressure)
390.0  /tinf    (freestream temperature)
 0.              0.1347191240328      0.
 2.6244059E-4    0.1132312733923      0.
 9.4530382E-4    7.0124557394367E-2   0.
 1.8810658E-3    4.6016691556783E-2   0.
 2.9971707E-3    3.1253217343323E-2   0.
 4.2705112E-3    2.1114260233283E-2   0.
 5.6953584E-3    1.3796344532341E-2   0.
 7.2747553E-3    8.3160311603793E-3   0.
 9.0147518E-3    4.0188934669989E-3   0.
 1.0925392E-2    5.4343477728721E-4   0.
 1.301854E-2    -2.1489054727016E-3   0.
 1.5307413E-2   -4.103024062921E-3    0.
 1.7803775E-2   -6.3038138624276E-3   0.
 2.0526798E-2   -8.4553393854651E-3   0.
 2.34928E-2     -9.8847372967642E-3   0.
 2.6720202E-2   -1.1098457423478E-2   0.
                     .
                     .
                     .
 0.9824749       2.3585518081544E-2   0.
 0.9865789       2.8966689722272E-2   0.
 0.9903595       3.5253108067807E-2   0.
 0.9938442       4.3951539866815E-2   0.
 0.9970505       5.3919871571419E-2   0.
 1.              6.5944987759235E-2   0.
```

Appendix B: Output Files

Outfile file "legend"

step	x*	del*/L*	delta*	Mach_u	rmax	imax
0	0.0000000E+00	0.1430674E+01	0.2222551E-03	0.0000000E+00	0.1350571E-07	6
2	0.1435503E-01	0.1763038E+01	0.3173347E-03	0.5206726E+00	0.2154925E-06	11
4	0.3125234E-01	0.2366497E+01	0.5700238E-03	0.6863386E+00	0.2066538E-06	13
6	0.5126869E-01	0.2689383E+01	0.8060416E-03	0.7568990E+00	0.3413945E-06	12
8	0.7498714E-01	0.2913725E+01	0.1041978E-02	0.7961337E+00	0.4411312E-06	11
10	0.1030743E+00	0.3100542E+01	0.1290048E-02	0.8208850E+00	0.1781216E-06	11
12	0.1362966E+00	0.3217949E+01	0.1532241E-02	0.8375850E+00	0.2482159E-06	7
14	0.1755287E+00	0.3329082E+01	0.1791834E-02	0.8520063E+00	0.1293438E-06	10
16	0.2217676E+00	0.3434735E+01	0.2072884E-02	0.8614153E+00	0.1185993E-06	9
18	0.2761402E+00	0.3506434E+01	0.2356517E-02	0.8695486E+00	0.1832802E-06	8
20	0.3399068E+00	0.3577373E+01	0.2663127E-02	0.8760325E+00	0.1388041E-06	8
22	0.4144507E+00	0.3632934E+01	0.2982440E-02	0.8814904E+00	0.2513429E-06	7
24	0.5012724E+00	0.3676531E+01	0.3315544E-02	0.8863561E+00	0.1103803E-06	7
26	0.6019561E+00	0.3718341E+01	0.3671124E-02	0.8904525E+00	0.4261433E-06	6
28	0.7181306E+00	0.3756340E+01	0.4047261E-02	0.8942131E+00	0.8833897E-07	7
30	0.8514025E+00	0.3767767E+01	0.4416550E-02	0.8979295E+00	0.8888528E-07	7
32	0.1003277E+01	0.3779752E+01	0.4805359E-02	0.9018746E+00	0.3266885E-06	5
34	0.1175043E+01	0.3792276E+01	0.5213497E-02	0.9055657E+00	0.8976225E-07	6
36	0.1367650E+01	0.3795478E+01	0.5624686E-02	0.9094002E+00	0.2393598E-06	6
38	0.1581563E+01	0.3789931E+01	0.6034509E-02	0.9135010E+00	0.4500929E-06	6
40	0.1816618E+01	0.3781879E+01	0.6447810E-02	0.9178708E+00	0.4005004E-06	6
42	0.2071904E+01	0.3774961E+01	0.6867179E-02	0.9222863E+00	0.4239713E-06	6
44	0.2345658E+01	0.3768265E+01	0.7287375E-02	0.9266923E+00	0.6726634E-07	7
46	0.2635245E+01	0.3762494E+01	0.7705623E-02	0.9310882E+00	0.3267236E-06	6
48	0.2937203E+01	0.3764590E+01	0.8133370E-02	0.9350821E+00	0.1027020E-06	5
50	0.3247372E+01	0.3767901E+01	0.8553584E-02	0.9387523E+00	0.2202283E-06	5
52	0.3561097E+01	0.3765214E+01	0.8945024E-02	0.9422244E+00	0.1433897E-06	7
54	0.3873515E+01	0.3783265E+01	0.9368727E-02	0.9451995E+00	0.3759408E-06	7
56	0.4179840E+01	0.3878009E+01	0.9974963E-02	0.9456833E+00	0.1965184E-06	7
58	0.4475640E+01	0.4109018E+01	0.1094322E-01	0.9424782E+00	0.1737138E-06	7

Outfile file "sta_0058"

```
3 /number of header records
0.44756403067253E+01 /x*
0.10943219324209E-01 /delta*
0.41090179017183E+01 -.17330631115000E+01 /dol, phi(deg)
42
 0.000000000000000E+00  0.100000000000000E+01  0.000000000000000E+00
0.2049257838884E+01 0.0000000000000E+00 0.0000000000000E+00 0.0000000000000E+00
0.1775266507739E-11 0.1499864395883E+00 0.1650165890827E+00 0.1870455205679E-13
-.4736774938549E-01 0.4235754057480E-01 -.1875125248799E-09 0.7175862211209E-03
 0.142881152183827E-01  0.100000128910483E+01 -0.526462043119655E-04
0.2049253001368E+01 0.2147348282272E-02 0.2357777379672E-02 0.7308298872691E-07
-.6773102823868E-03 0.1505918742467E+00 0.1650168731993E+00 0.1021837297079E-04
-.4743991377321E-01 0.4238739313721E-01 0.4042780866942E-04 0.7127460511339E-03
   .
   .
   .
 0.145894283155801E+02  0.100131628995567E+01  0.260143956494611E+01
0.1000000000000E+01 0.1000000000000E+01 0.1000000000000E+01 0.4387097619112E-02
-.1587864062458E-08 -.3296918293927E-11 -.7673861546209E-11 0.4498749479165E-05
0.3458531461220E-08 -.3245992363787E-10 -.7122808454163E-09 -.8246321650703E-09
   27                   /no. of trailer records
 0.447564030672532E+01 /x*
 0.657951999999998E+00 /l*/c*
 0.951042244770178E-02 /t*/c*
-0.173306311149996E+01 /phi (deg)
 0.109432193242091E-01 /displacement thickness*
 0.410901790171832E+01 /delta*/L*
 0.248885825547478E+01 /edge total Mach no.
 0.942478246658577E+00 /edge u Mach no.
 0.230350823102943E+01 /edge w Mach no.
 0.631016966003098E+06 /edge unit Reynolds no.*
 0.282420496727099E+07 /edge Re no. based on x*
 0.168053710678193E+04 /edge Re no. based on L*
 0.690535705626887E+04 /edge Re no. based on delta*
 0.894399863413379E+03 /edge u-velocity*
 0.000000000000000E+00 /wall v-velocity*
 0.218600000000920E+04 /edge w-velocity*
 0.130386856151895E+03 /edge pressure*
 0.202694083069417E-03 /edge density*
 0.374865488202295E+03 /edge temperature*
 0.768196040225634E+03 /wall temperature*
 0.287297442032797E-06 /edge viscosity*
 0.140000000000000E+01 /gamma
 0.719999999999999E+00 /Prandtl number
 0.227000000000000E-07 /first Sutherland constant*
 0.198600000000000E+03 /second Sutherland constant*
 0.171600000000000E+04 /ideal gas constant*
 0.173713816664645E-06 /rmax
```

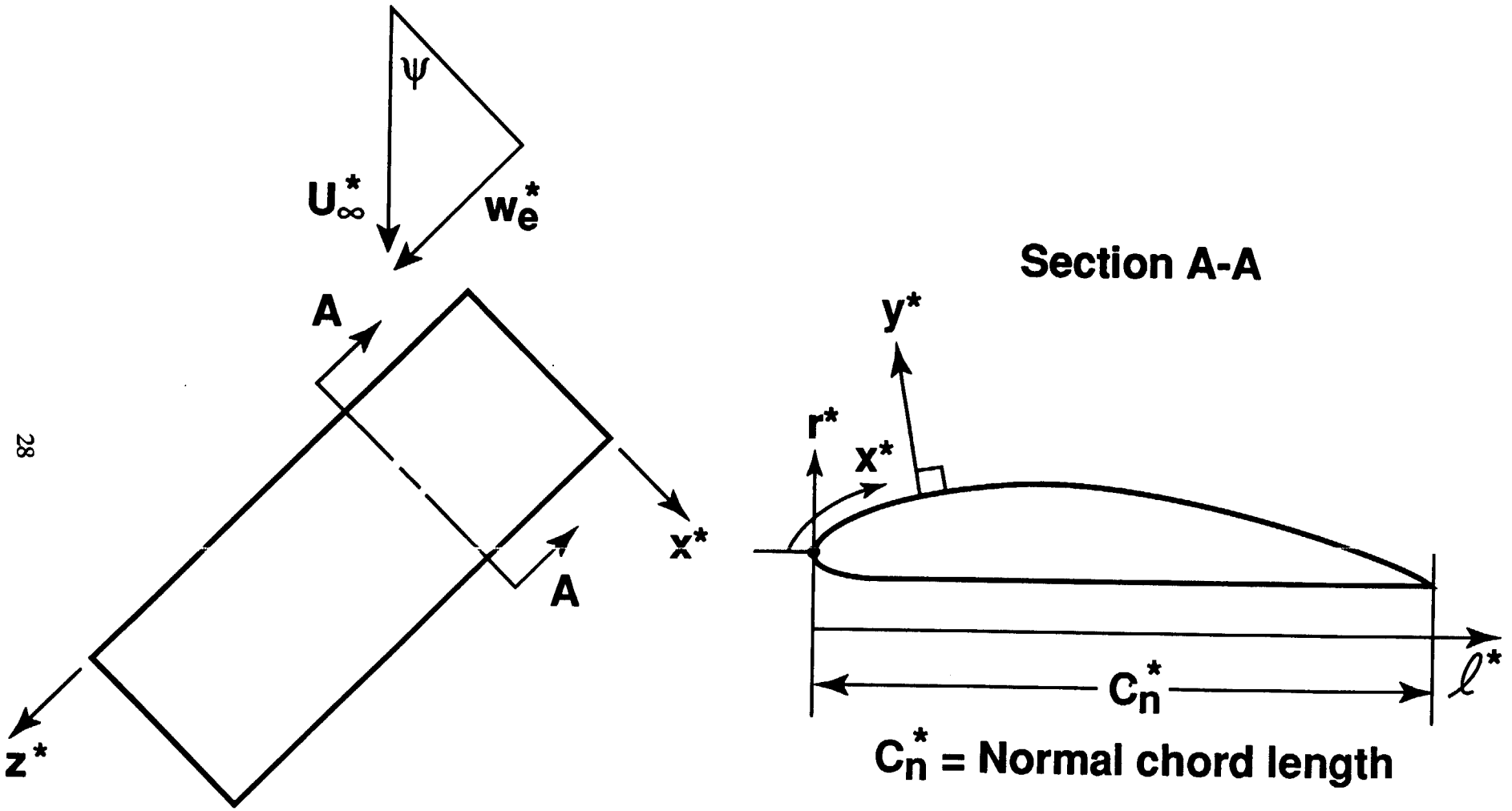

Figure 1: Geometry and coordinate system.

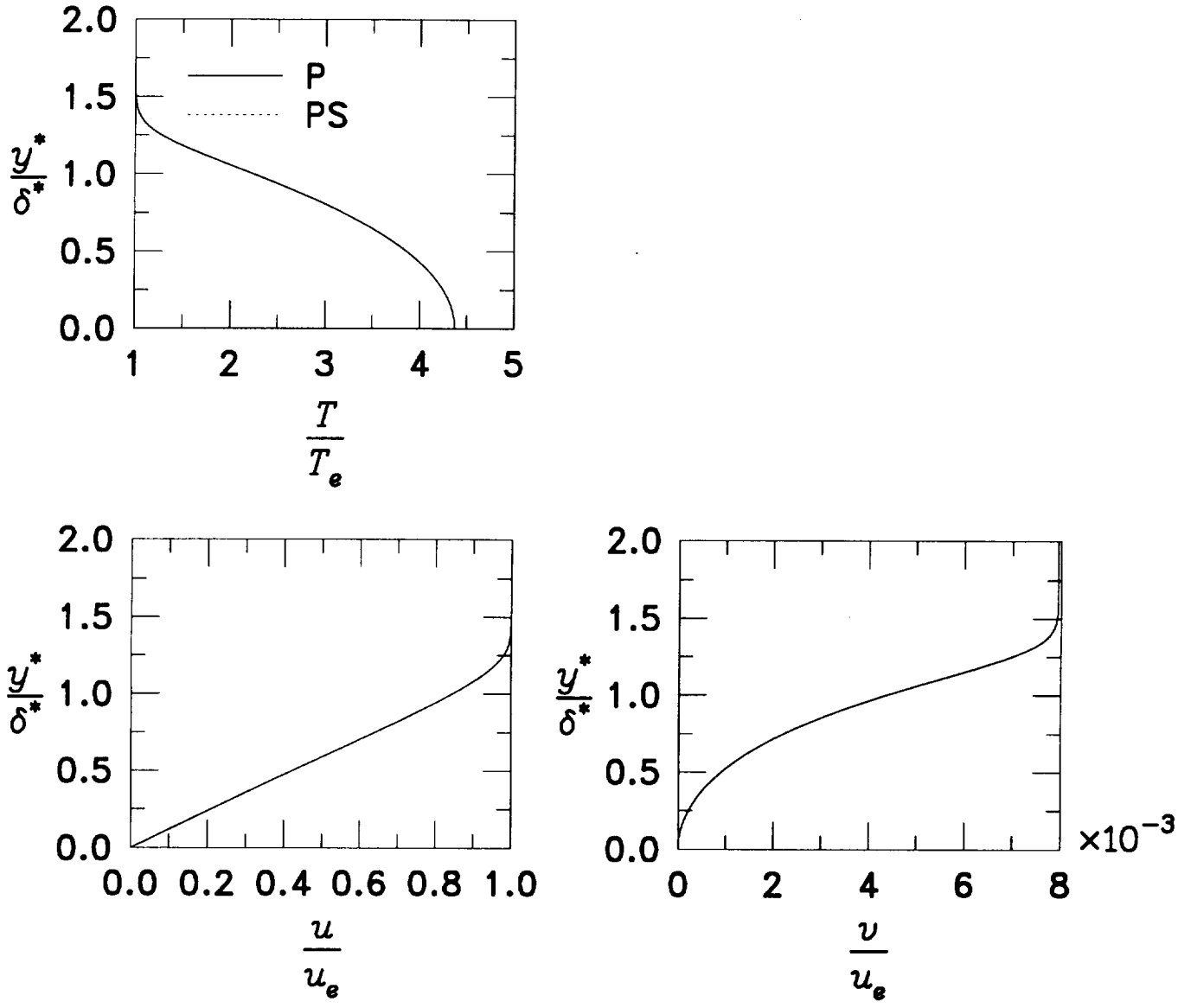

Figure 2: Comparison of present results (P) with those of Pruett and Streett (PS) for two-dimensional Mach 4.5 flow over insulated flat plate.

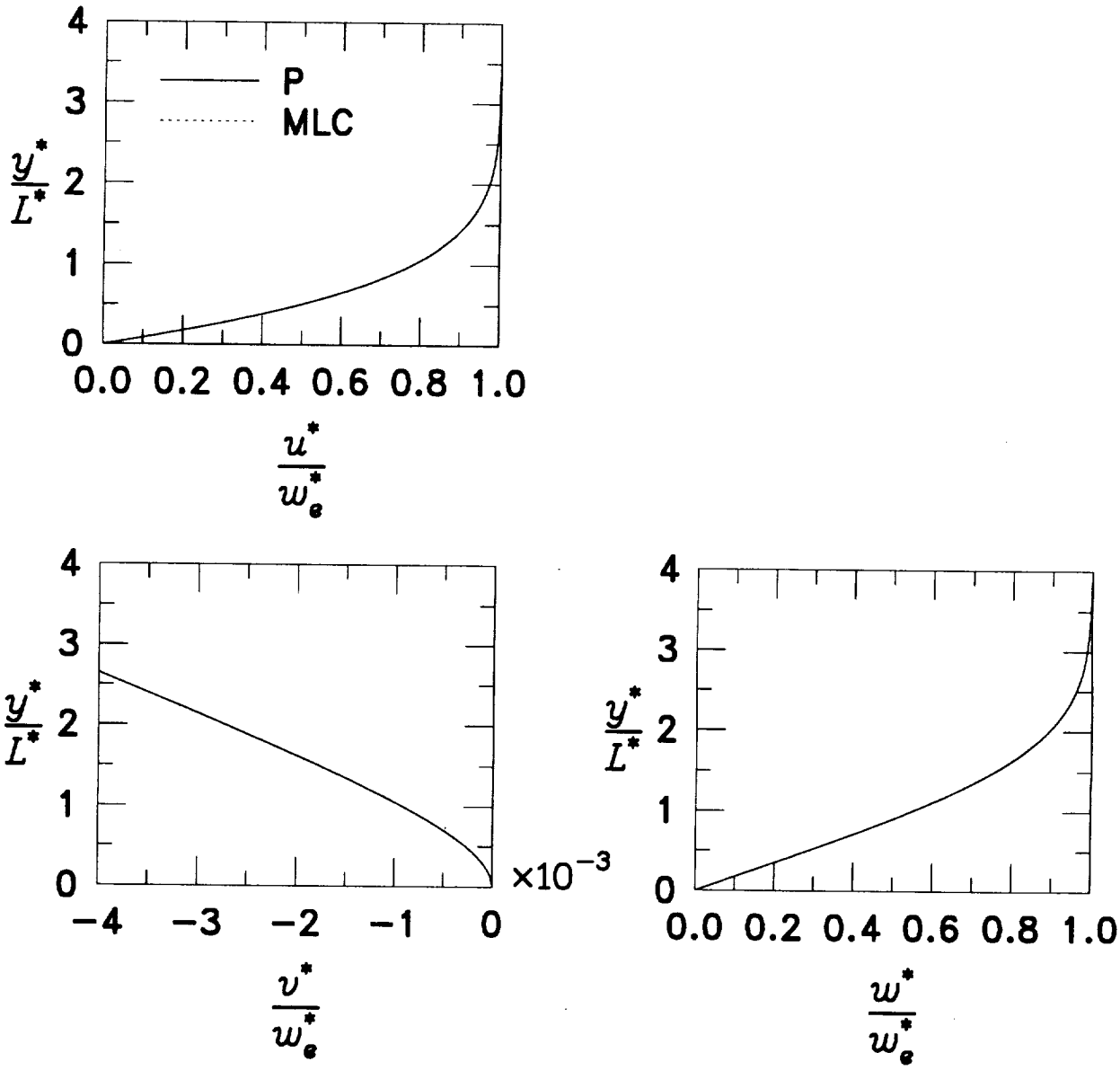

Figure 3: Comparison of present results (P) with those of Malik et al. (MLC) for incompressible swept Hiemenz flow.

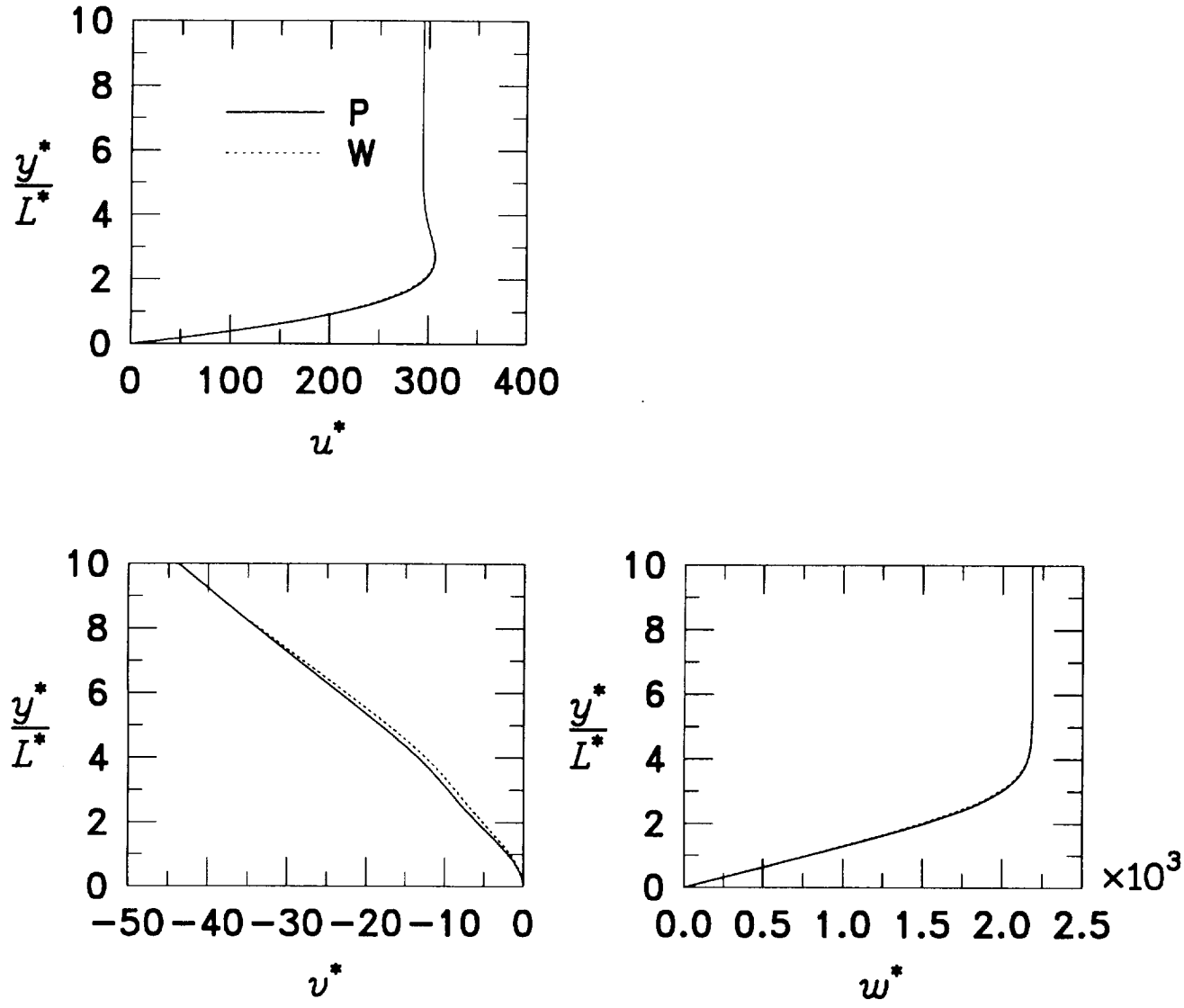

(a) $l^*/c^* = 0.001$.

Figure 4: Comparison of velocities obtained by present method (P) with results obtained from Wie's (W) code for highly swept wing in Mach 2.4 flow.

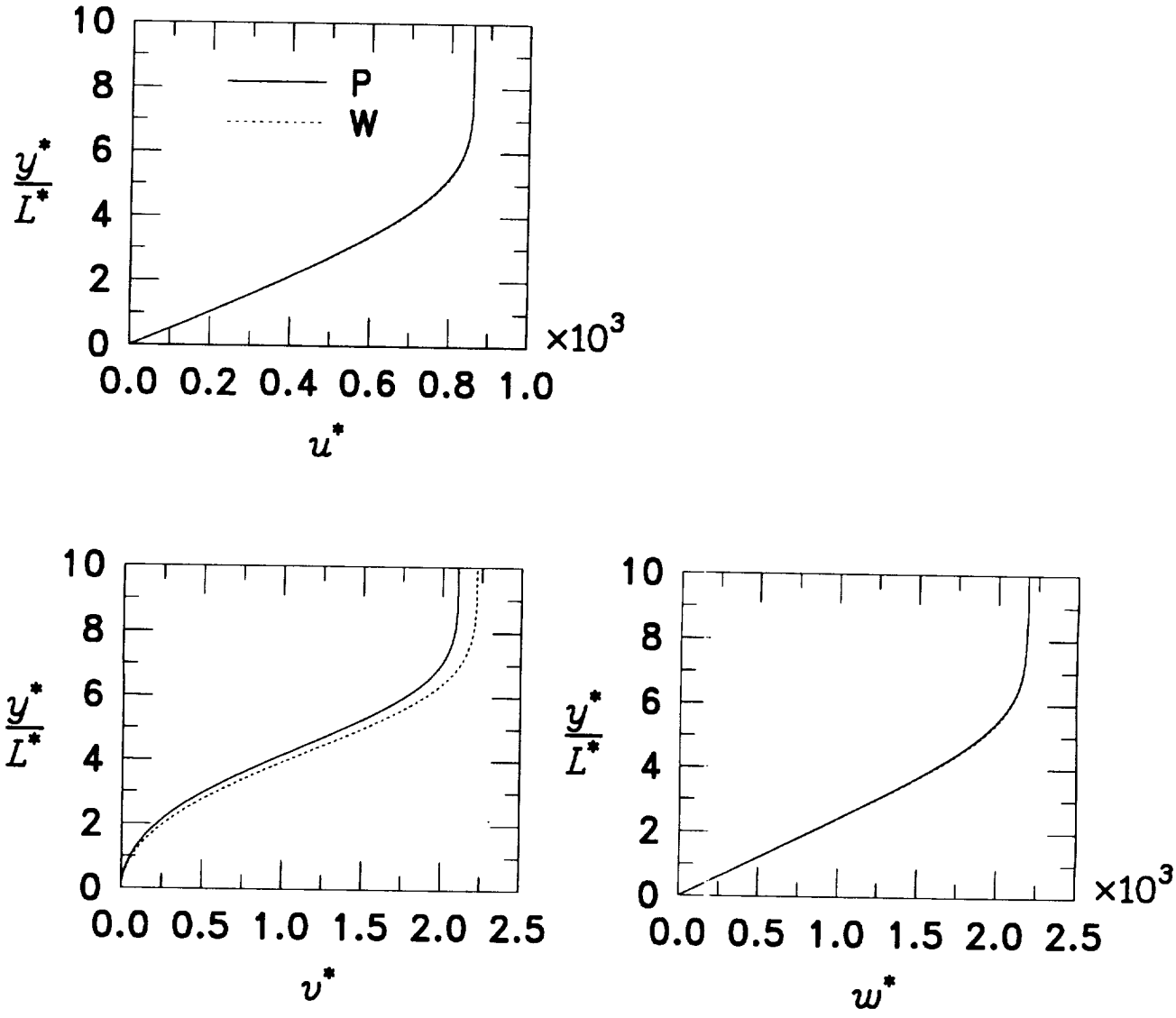

(b) $l^*/c^* = 0.126$.

Figure 4: Continued.

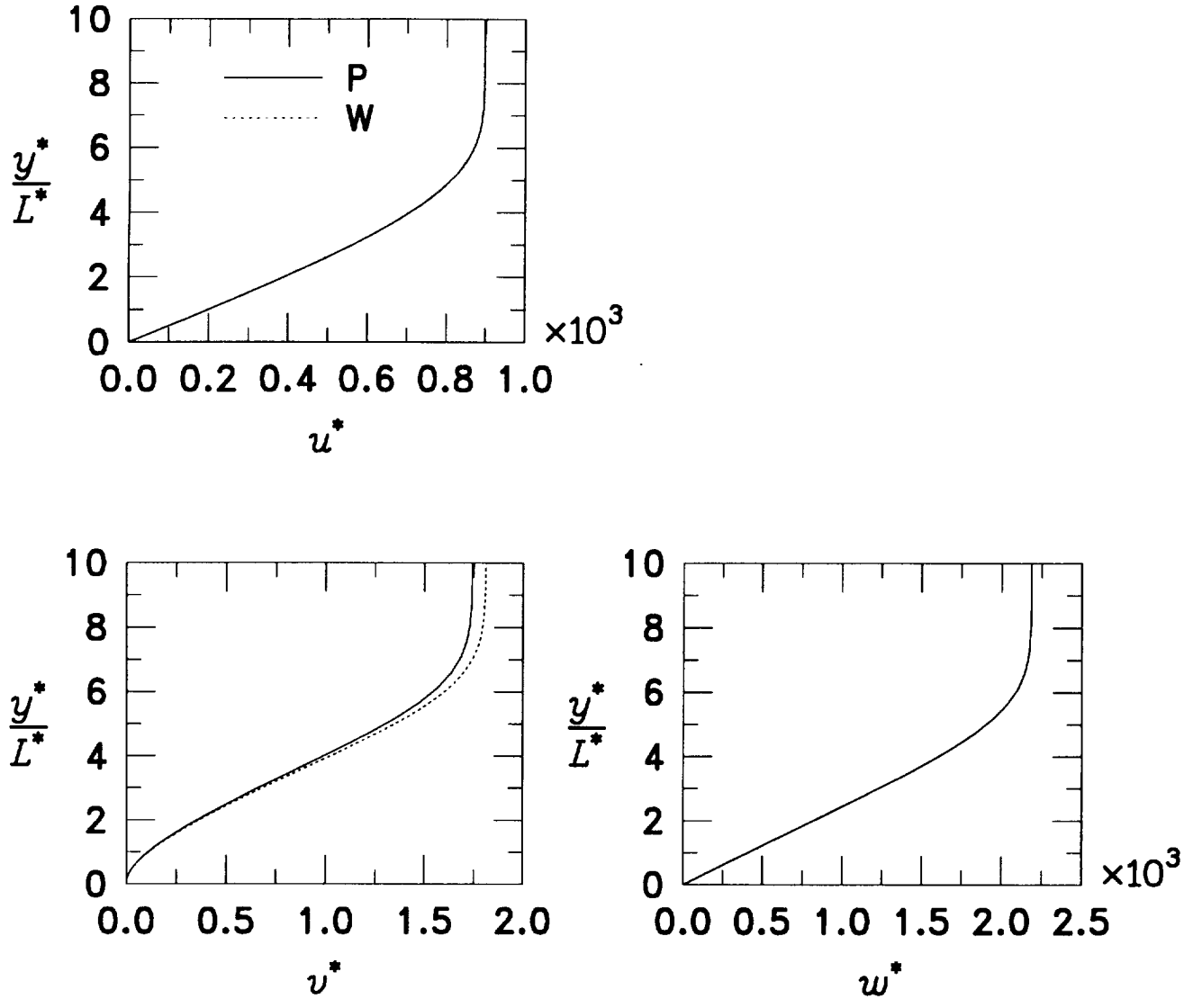

(c) $l^*/c^* = 0.595$.

Figure 4: Concluded.

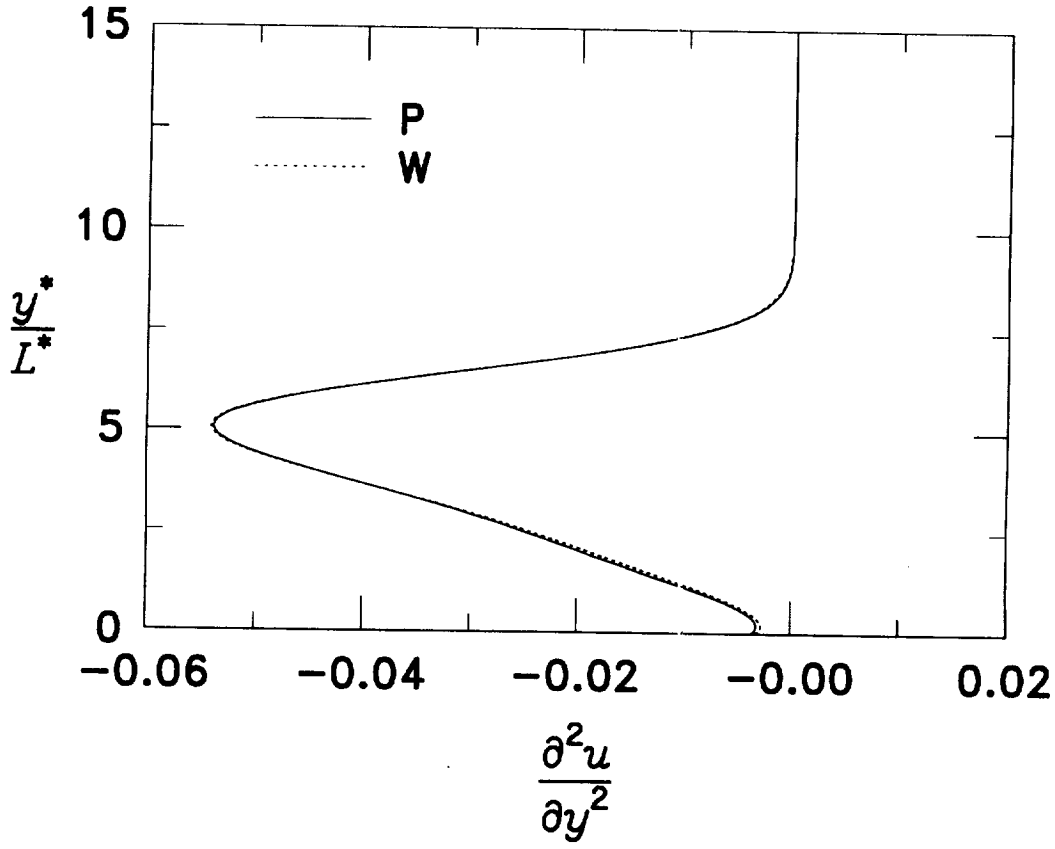

Figure 5: Comparison of $\frac{\partial^2 u}{\partial y^2}$ from present method (P) with that obtained from Wie's (W) code for highly swept wing in Mach 2.4 flow with $l^*/c^* = 0.595$.

REPORT DOCUMENTATION PAGE

Form Approved
OMB No. 0704-0188

1. AGENCY USE ONLY (*Leave blank*)	2. REPORT DATE	3. REPORT TYPE AND DATES COVERED
	December 1994	Contractor Report

4. TITLE AND SUBTITLE
A Spectrally Accurate Boundary-Layer Code for Infinite Swept Wings

5. FUNDING NUMBERS
C NAS1-19656
WU 505-59-50-02

6. AUTHOR(S)
C. David Pruett

7. PERFORMING ORGANIZATION NAME(S) AND ADDRESS(ES)
The College of William and Mary
Williamsburg, VA 23185

8. PERFORMING ORGANIZATION REPORT NUMBER

9. SPONSORING / MONITORING AGENCY NAME(S) AND ADDRESS(ES)
National Aeronautics and Space Administration
Langley Research Center
Hampton, VA 23681-0001

10. SPONSORING / MONITORING AGENCY REPORT NUMBER
NASA CR-195014

11. SUPPLEMENTARY NOTES
Langley Technical Monitor: C. L. Streett
Interim Report

12a. DISTRIBUTION / AVAILABILITY STATEMENT
Unclassified - Unlimited

Subject Category - 34

12b. DISTRIBUTION CODE

13. ABSTRACT (*Maximum 200 words*)

This report documents the development, validation, and application of a spectrally accurate boundary-layer code, WINGBL2, which has been designed specifically for use in stability analyses of swept-wing configurations. Currently, we consider only the quasi-three-dimensional case of an infinitely long wing of constant cross section. The effects of streamwise curvature, streamwise pressure gradient, and wall suction and/or blowing are taken into account in the governing equations and boundary conditions. The boundary-layer equations are formulated both for the attachment-line flow and for the evolving boundary layer. The boundary-layer equations are solved by marching in the direction perpendicular to the leading edge, for which high-order (up to fifth) backward differencing techniques are used. In the wall-normal direction, a spectral collocation method, based upon Chebyshev polynomial approximations, is exploited. The accuracy, efficiency, and user-friendliness of WINGBL2 make it well suited for applications to linear stability theory, parabolized stability equation methodology, direct numerical simulation, and large-eddy simulation. The method is validated against existing schemes for three test cases, including incompressible swept Hiemenz flow and Mach 2.4 flow over an airfoil swept at 70° to the free stream.

14. SUBJECT TERMS			15. NUMBER OF PAGES
Compressible Coundary Layer Equations Swept Wings Three-Dimensional Boundary Layers		Spectral Methods	35
			16. PRICE CODE A03
17. SECURITY CLASSIFICATION OF REPORT	18. SECURITY CLASSIFICATION OF THIS PAGE	19. SECURITY CLASSIFICATION OF ABSTRACT	20. LIMITATION OF ABSTRACT
Unclassified	Unclassified	Unclassified	